Laboratory modelling of momentum transport by internal gravity waves and eddies in the Antarctic circumpolar current

Joël Sommeria, Adekunle-Opeoluwa Ajayi, Keshav Jayakrishnan Raja, Chantal Staquet, Samuel Viboud, Bruno Voisin

Laboratory modelling of momentum transport by internal gravity waves and eddies in the Antarctic circumpolar current

Joel Sommeria, Adekunle-Opeoluwa Ajayi, Keshav J. Raja, Chantal Staquet, Samuel Viboud, Bruno Voisin

Laboratoire des Ecoulements Geophysiques et Industriels (LEGI)
CNRS, Universite Grenoble Alpes, France
joel.sommeria@legi.cnrs.fr

Abstract

The Antarctic Circumpolar current is recognized as a key location for ocean mixing, and its interaction with the bottom topography is an important source of energy dissipation and mixing. We have reproduced this process in a linearly stratified fluid on the Coriolis rotating platform, 13 m in diameter. A uniform circular current around the tank is produced by a small change of tank rotation speed (spinup) which persists by inertia for the duration of the experiment. The wake of a single spherical cap is first investigated, involving wave emission and vortex shedding. Then a bottom roughness is introduced as a set of 18 spherical caps. In the absence of background rotation, the friction effect on the current is mainly confined to the wake located below the topography top, with a weak contribution of the radiated lee waves. By contrast, the background rotation favors the downward transport of momentum by mechanisms that we relate to the excitation of inertial waves and Ekman pumping enhanced by the rough bottom.

1 Introduction

The Antarctic Circumpolar current is recognized as the main source of ocean mixing with strong impact on Earth climate. Recent field campaigns in the Southern Ocean (Naveira-Garabato et al. (2004)) have revealed that the interaction of this current with bottom topography can radiate internal gravity waves whose momentum transport contributes to friction. This process has been theoretically studied by Nikurashin and Ferrari (2010) and Labreuche et al. (2016) with an idealised 2D topography.

However a 3D topography behaves differently, because the fluid can flow horizontally around as well as rising above it, thus generating a lee wave. This happens if the Froude number $\mathrm{Fr} = U_0/(Nh)$ is smaller than 1, which means that the flow has not enough kinetic energy to rise over the topography of height h (here U_0 is the upstream velocity and N the buoyancy frequency). Then a vortical wake is produced, with the possibility of periodic vortex shedding, as nicely observed in the atmospheric wakes behind islands (Etling (1990)).

The competition between the vortical wake and the lee wave can be estimated by the empirical concept of dividing streamline of Sheppard (1956): this streamline is at the vertical level such that the remaining height h_s of the cap above corresponds to a Froude number $U_0/(Nh_s)$ equal to 1: in other words it is defined by $h_s/h = \mathrm{Fr}$ (for $\mathrm{Fr} < 1$). The fluid above this dividing streamline flows over the topography, exciting a lee wave, while the fluid below it flows around with quasi-horizontal motion. For $Fr > 1$ the whole topography height h is involved in the wave emission. This problem has been much studied in the context of atmospheric dynamics, and several laboratories experiments in

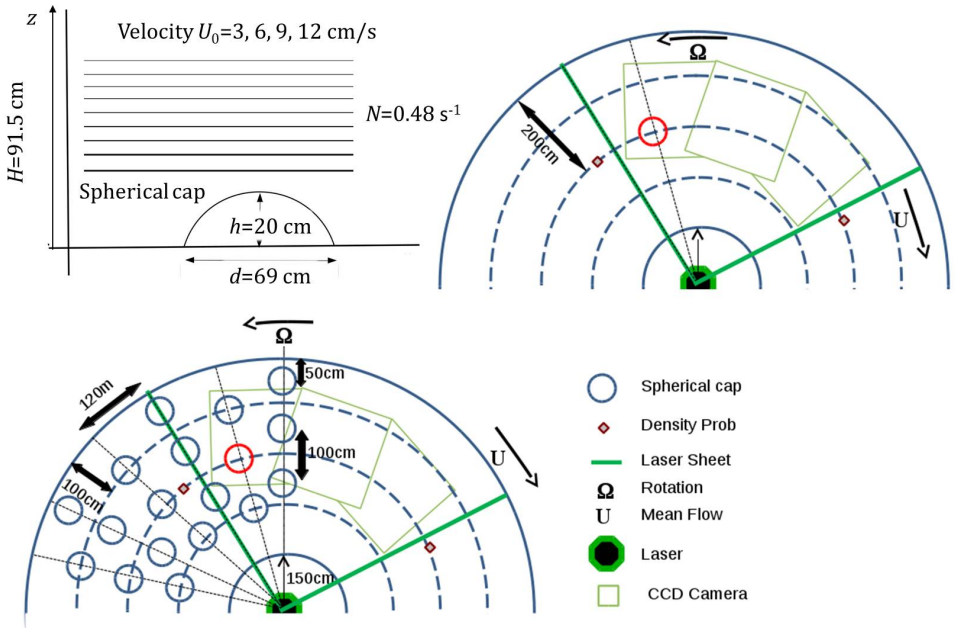

Figure 1: Sketch of the experimental set-up. The topography shape with a typical set of laser sheet levels is sketched in the upper left view. The single cap configuration is sketched in the upper right, showing the laser sheet, the view fields of the three cameras and the probe positions. The multi-cap configuration is sketched in the lower view.

a linearly stratified fluid have been performed, for instance Baines (1995), Dalziel et al. (2011). However few studies involve the Coriolis effect.

2 Experimental set-up

The cylindical tank of the 'Coriolis' platform, 13 m in diameter, is filled with water linearly stratified in density by salinity, up to a total height H=91.5 cm. A uniform circular current is produced by a small sudden change of the tank rotation speed (spinup). This circular current persists by inertia for the duration of the experiment, typically 15 minutes, over which the flow conditions can be considered quasi-steady. A spherical cap is fixed on the flat horizontal bottom of the tank, centered at a distance 2 m from the tank edge (at radius r_0=4.5 m from the tank centre) such that the lateral confinement of the wake is marginal. The cap has a height h=20 cm and a diameter d=69 cm at its basis, see figure 1. It is cut from a sphere of radius R=40 cm. The buoyancy frequency is set to N=0.48 s^{-1} in all the experiments (corresponding to $\delta\rho/\rho$=2.15 % over the water height H). The multiple cap experiments are done in a similar way with a pavement of 18 identical caps as sketched in the lower part of figure 1.

The 'non-rotating' case (f=0) is obtained by suddenly starting the tank rotation at angular speed $\Delta\Omega$ (anticlockwise), while the water remains at rest by inertia, yielding a clockwise fluid velocity in the reference frame of observation. The fluid velocity $U_0 = r_0\Delta\Omega$ produced above the cap is set to 3, 6, 9 or 12 cm/s, such that the Froude number $\mathrm{Fr} = U_0/(Nh)$ takes the values 0.31 to 1.25 (see Table 1).

The 'rotating' case is similarly obtained by first preparing the stratified water layer with a tank rotation at a constant angular velocity Ω=0.095 rd/s (0.9 turns/minute). This

yields a Coriolis parameter $f = 2\Omega$=0.19 s^{-1}, so that f/N=0.4. At the experiment start t=0, the tank velocity is suddenly increased by the amount $\Delta\Omega$ producing a clockwise fluid rotation in the reference frame like in the non-rotating case.

Vertical density profiles are measured before and during the experiment by two motorised profilers equipped with conductivity probes. Velocity fields are measured by Particle Imaging Velocimetry in horizontal planes with three cameras covering a field of width 2 m centered at the radius r_0=4.5 m of the reference cap, spanning a quarter of the periphery, see figure 1. The flow is illuminated by a laser sheet, produced by a rapidly oscillating mirror (100 Hz) from a 6 watt continuous Yag laser located at the tank centre. The laser sheet is vertically scanned at 10 successive heights z, repeated in a periodic way. A set of 100 images (during typically 25 s) is obtained at each level. Each experiment is reproduced twice to scan either the lower wake either the upper layers where waves propagate. A few experiments with a fixed laser position are also performed to get continuous time series. The fluid is seeded by polystyrene particles of diameter 0.2 mm sorted in density to provide a uniform concentration at different heights.

The Antarctic Circumpolar Current is characterised by a buoyancy frequency N=7 10^{-4} s^{-1} and a velocity U_0=10 cm/s in the deep ocean and a Coriolis parameter f=1.5 10^{-4} s^{-1}, so that f/N=0.2 (see e.g. Nikurashin et al. (2013)). Our range of Froude numbers 0.31 to 1.25 then corresponds to a topographic height $h = U_0/(NFr)$ in the range 460-115 m, and a base diameter 1600-400 m, if we keep the same aspect ratio d/h=3.5. Accounting for the ratio f/N twice lower than the experiment, a better similarity is however expected for a twice flatter topography, with base diameter 3200-800 m. Indeed the ratio $(f/N)(d/h)$ is generally the relevant similarity parameter to compare situations with different aspect ratios (this is exact within the hydrostatic approximation). Our experiments with rotation are therefore representative of the effect of circular sea mounts a few kilometers in diameter and a few hundred meters in height. The Reynolds number U_0h/ν is in the range 0.6-2.4 10^4, which is of course smaller that in the ocean but sufficient to get instabilities and turbulent processes.

3 Wave emission

As expected, lee waves are observed on horizontal cuts made at altitudes z above the cap top $z = h$=20 cm, as shown in figure 2, where the stream-wise velocity is represented. The case without rotation (left hand side) and with f/N=0.4 (right hand side) are compared, other parameters being the same. The maps are made with polar coordinates rescaled to approach a cartesian geometry, hence straightening the curved streamlines associated with the circular flow around the tank. Thus x is the clockwise angular displacement with respect to the cap centre rescaled by its reference radius r_0=4.5 m, while $y = r - r_0$ is the shifted radius. A reference velocity is subtracted to the azimuthal velocity to extract the wave oscillations from the mean flow. This reference is obtained at each radius as the upstream velocity measured at x=-72 cm (it increases linearly with radius r).

The wave pattern is set after typically 100 s (the time of advection through the measured field for the smallest velocity U_0=3 cm/s), and it then remains quasi-steady during the whole experiment. Fluctuations however occur in association with the turbulence produced in the lower wake, so the fields of figure 2 are averaged over 25 s to better display the wake structure. The mean velocity profile remains uniform during a time $2\pi r_0/U_0$

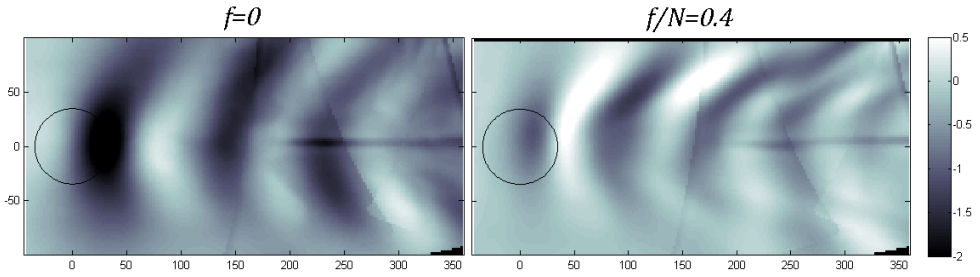

Figure 2: Horizontal cut showing the lee wave as a color map of the stream-wise velocity, left, no rotation, right, f/N=0.4. U_0=6 cm/s, height z=41 cm, time t=165-190 s (fields are averaged over 25 s to reduce fluctuations). The horizontal line is due to the wake of a density probe while oblique lines mark the boundaries between the three camera views

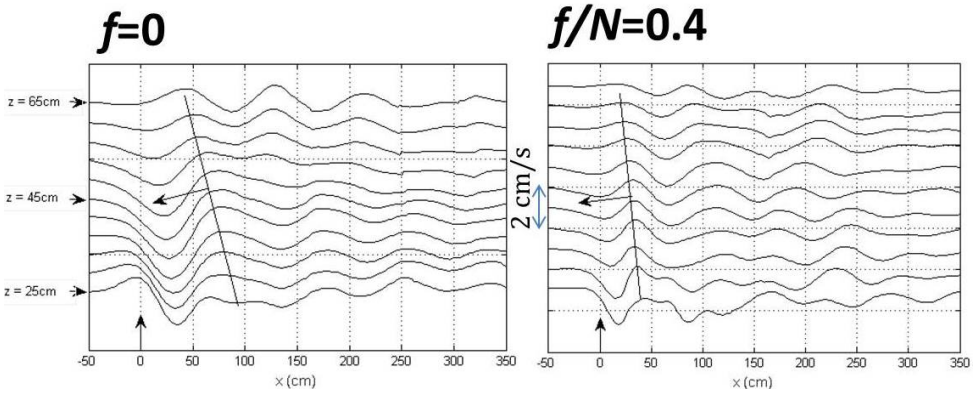

Figure 3: Profiles of the stream-wise velocity component along x at different levels z, left, no rotation, right, f/N=0.4. U_0=6 cm/s. The time t is ranging from 300 s to 570 s from top to bottom. The velocity is averaged in the range y=-17 to +17 cm. Curves are shifted by 1 cm/s to distinguish the different levels. The dominant wave crest and perpendicular wave vector (arrow) are sketched.

(equal to 500 s for U_0=6 cm/s), after which the lower velocity is perturbed upstream by the return of the wake perturbations after one revolution around the tank. Therefore the main measurements are performed in the time range 100-500 s. The wake structure in

the absence of rotation is in reasonable agreement with the linear theory of Voisin (2007) for the wave emission of a spherical cap emerging from the horizontal plane of the dividing streamline defined above. However significant nonlinear effects already occur even at the lower Froude number investigated (Fr=0.31 for U_0=3 cm/s).

In the case of background rotation no theory has been published to our knowledge. An asymmetry between the two sides is clearly visible in this case, with a stronger wake observed for $y > 0$ (figure 2 right). This can be understood by the following argument: a fluid element impinging on the cap at $y > 0$ is first deviated away with positive transverse velocity v, then goes back to 0 with a positive stream-wise velocity perturbation u (due to the lateral squeezing of the streamlines), and then comes back with $v < 0$. The velocity vector rotates clockwise in this process which fits with the natural behaviour of the inertio-gravity wave. The opposite rotation is forced on the other side, explaining the less efficient wave generation.

Table 1: Horizontal wavelengths λ measured for increasing velocities U_0, no rotation. The angle θ of the wavevector deduced from the intrinsic frequency $\tilde{\omega} = 2\pi U_0/\lambda$ is deduced, using the dispersion relation $\cos\theta = \tilde{\omega}/N$. The Froude number $\mathrm{Fr} = U_0/(hN)$, the estimated height $h_s = \mathrm{Fr}\ h$ and the corresponding diameter $d_s = 2\sqrt{(2R - h_s)h_s}$ over the dividing streamline are also indicated.

U_0	λ **(cm)**	θ **(degrees)**	**Fr**	h_s**(cm)**	d_s**(cm)**
3	46	31	0.31	6.25	43
6	86	24	0.62	12.5	58
9	125	23	0.94	18.7	68
12	170	22	1.25	20	69

The dominant wavelength can be determined by the distance between the two first minima on the stream-wise velocity profiles, as shown in figure 3. It increases with increasing speed, as shown in Table 1. This increase can be partly explained by the widening of the cap of height h_s which effectively emits the wave, according to the dividing streamline argument. Its diameter d_s is also shown in Table 1. However the ratio λ/d_s also increases with the Froude number, which shows that nonlinear effects are at stake. For the highest Froude numbers, a turbulent wake is produced over a height $\sim h$ behind the obstacle and the wave emission occurs at the interface of this wake rather than at the obstacle itself.

The intrinsic frequency $\tilde{\omega} = (2\pi/\lambda)U_0$ can be determined from the data of Table 1. It turns out to remain close to N for each of the experiments, so that the wave vector is close to horizontal. The angle θ of the wave-vector with respect to the horizontal, obtained by the dispersion relation $\tilde{\omega}/N = \cos\theta$, is displayed in Table 1.

4 Wake of eddies

The lower part of the fluid is blocked by the cap, resulting in a wake laterally delimited by two bands of opposite vorticity, as visualized in figure 4. In the absence of rotation (left hand side), the wake is fairly straight. By contrast, the background rotation favors a flow organisation into a Karman vortex street (right hand side) with periodic shedding of coherent vortices.

The Strouhal number $S = f_s d_m/U_0$ can be calculated from the measured shedding frequency f_s and the obstacle diameter d_m=54 cm taken at z=10 cm, mid-height of the cap. With this definition we find that S=0.20 for both cases U_0=3 cm/s and U_0=6 cm/s, which corresponds to the usual vortex shedding in the wake of a cylinder. For higher values of the velocity, Fr $>$ 1, the periodic shedding disappears. Then the dividing streamline

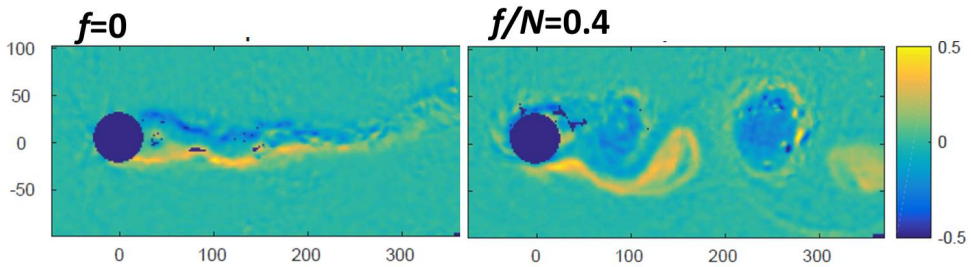

Figure 4: Color map of the vertical vorticity component (in s^{-1}) in the wake region, horizontal cut at z=10 cm, left, no rotation, right f/N=0.4. U_0=3 cm/s, time t=400 s.

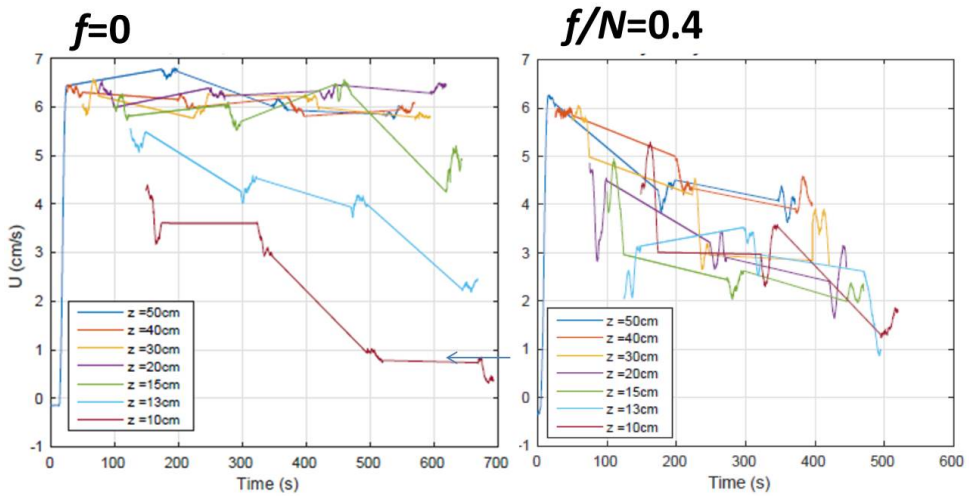

Figure 5: Decay of the stream-wise velocity in the multi-cap case, left, no rotation, right, f/N=0.4. The velocity is averaged in the range y=[-0.5 0.5] m and x=[2.5 3.5] m. At each level z, the curve is made of discontinuous set of time series measured when the laser sheet is positioned at this level, joined by straight lines.

reaches the tank bottom $z = 0$, so that the whole obstacle height is involved in wave emission, with no remaining quasi 2D layer vortex shedding.

5 Global friction effect

We analyse in a similar way the effect of a pattern of 18 identical caps in an attempt to reproduce the effect of a random topography. Lee waves and vortices shed by each cap interact in a complex way, and we here discuss the global effect on the mean flow. We measure the mean stream-wise velocity in a domain 1 x 1 m^2 centered at y=0 and x=3 m, about 2 m away from the last caps to avoid local effects. The decay of this mean velocity at different levels z is shown in figure 5.

In the absence of rotation (left hand side), the velocity is observed to decay at the lowest level z=10 cm first, then to the levels z=13 and 15 cm. The flow remains quasi-unchanged above the topography top, so the bottom friction effect hardly penetrates upward. The behaviour with background rotation is different, with a similar decay at each level at least in the early stage up to t=300 s, showing that the bottom friction is efficiently transfered to the whole water column. An exponential decay time τ=500 s can be deduced from the plot. The decay however stalls in the upper layers in the late stage (t >300 s).

Low frequency oscillations develop over the main decay as shown in figure 6. Those contain a significant contribution of inertial oscillations, with amplitude about 0.25 cm/s, extracted in the lower graph of the figure by band-pass filtering of the signals (velocity components averaged in the 1x1 m^2 domain) around the inertial frequency $f/(2\pi$ (in Hz). The two velocity components oscillate in quadrature with u_x in advance of a quarter period with respect to u_y, as expected for inertial oscillations. This provides a support for the mechanism of inertial wave excitation by the lee waves proposed by Labreuche et al. (2016).

However this mechanism is not sufficient to explain the observed decay, as it can be

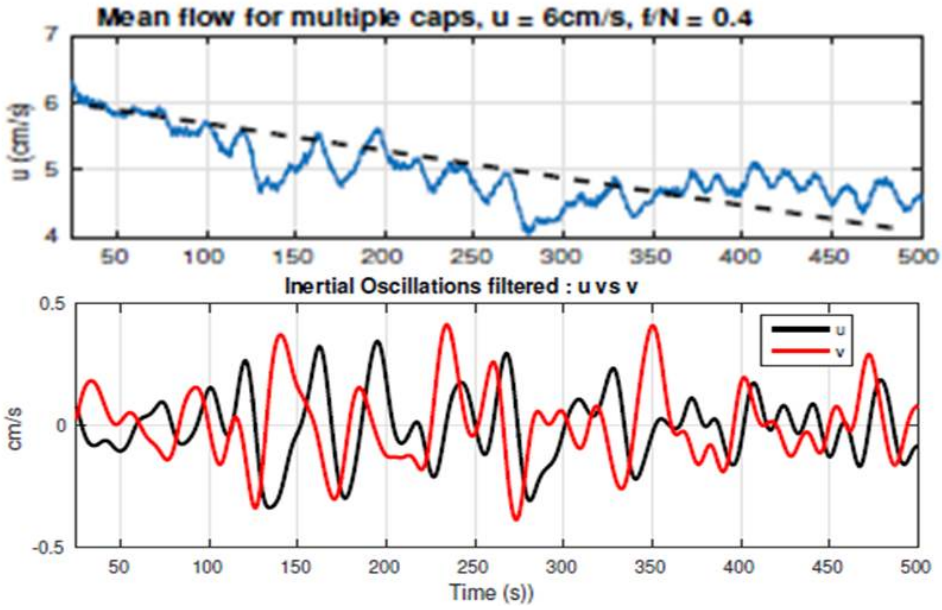

Figure 6: Top graph: decay of the stream-wise velocity in the multi-cap case, left, f/N=0.4, measured at level z=60 cm, averaged in the range y=[-0.5 0.5] m and x=[2.5 3.5] m. The oscillations of the u_x and u_y velocity components are displayed in the lower graph, obtained from the original signal after removing the linear trend (dashed line in the top graph) and filtering around the inertial frequency $f/(2\pi)$.

concluded by an analysis of the equation for the spatially averaged azimuthal velocity integrated from z_0 to H,

$$\frac{\mathrm{d}}{\mathrm{d}t}\int_{z_0}^{H} < u_x > \mathrm{d}z =< u_z u_x > + f\int_{z_0}^{H} < u_y > \mathrm{d}z \qquad (1)$$

In the absence of Coriolis effect, the observed decay would correspond to $H < u_x > /\tau \simeq < u_z u_x >$. This includes wave transport of momentum. From the experimental values H=91.5 cm, $< u_x >$=6 cm/s, τ=500 s, we deduce that $< u_z u_x > \simeq 1$ cm^2 /s^2. We do not measure the vertical velocity component u_z, but we expect it to be smaller than the horizontal velocity fluctuations, of the order 1 cm/s in the most active region behind the caps, covering a quarter of the tank periphery. The mean Reynolds stress $< u_z u_x >$, averaged over the tank periphery, is then definitely less than 0.25 cm^{2}s^{-2}, which is not enough to explain the observed decay.

The Coriolis term $f < u_y >$ must be therefore invoked. The observed decay can be explained by the Coriolis force acting on a transverse (radial) velocity $< u_y > = < u_x > /(\tau f) \simeq 0.06 cm/s$, uniform in the vertical the bulk region. It corresponds to an Ekman pumping effect. Since the vertical integral of the radial velocity must vanish by volume conservation, this means that an effective wall friction $u_*^2 = f\int_{z_0}^{H} < u_y > \mathrm{d}z \simeq 1$ cm^{2}s^{-2} should occur (here z_0 is close to 0 but above the Ekman layer). The laminar Ekman friction provides a wall stress $u_*^2 = \sqrt{\nu f/2} < u_x > \simeq 0.2$ cm^{2}s^{-2} (kinematic viscosity $\nu = 10^{-2}$ cm^{2}s^{-1}). The Ekman layer is unstable for a bulk velocity U such that the Reynolds number $\mathrm{Re}_\delta = U/\sqrt{\nu f/2}$ exceeds a threshold of 55, which corresponds to u=2 cm/s in our experiment. The velocity u=6 cm/s is above this threshold but it is still in the transitional regime with an Ekman friction close to the laminar value (Sous et al. (2013)).

The friction is however enhanced by the wake of the caps. Each cap is expected to provide a turbulent friction force $C_D h d u^2/4$, where C_D is a drag coefficient with a value close to 1 (and $hd/2$ is an estimate of the cross-flow section area). A pavement of caps with surface density n therefore provides an effective wall friction

$$u_*^2 = nC_D(hd/4)u^2 \tag{2}$$

Our caps are spaced by 1 m, but they cover a quarter of the tank periphery, so that the mean value is $n = 0.25$ m^{-2} $= 0.25\ 10^{-4}$ cm^{-2}. With a perfect arrest of the flow $C_D = 1$, this yields a friction force $u_*^2 = 0.3$ cm^{2}s^{-2}, 3 times lower than the measured one. However the turbulence induced in the wake is expected to trigger turbulence in the Ekman boundary layer which enhances friction.

Finally the Ekman pumping must be eventually blocked by stratification as heavy fluid is raised by the ascending motion. This results in a blocking of the Ekman friction in the upper part of the layer, as observed at the late stage ($t >$300 s). The resulting vertical shear can be a source of baroclinic instability which should develop on longer time scales.

References

Baines, P. G. (1995). Topographic Effects in Stratified Flows. *Cambridge University Press*.

Dalziel, S. B., Patterson, M. D., Caulfield, C. P., and LeBrun, S. (2011). The structure of low-Froude number lee waves over an isolated obstacle. *J. Fluid Mech.*, 689:3–31.

Etling, D. (1990). Mesoscale vortex shedding from large islands: a comparison with laboratory experiments of rotating stratified flows. *Met. and Atmos. Phys.*, 43:145–151.

Labreuche, P., Le Sommer, J., and Staquet, C. (2016). Enegy pathway of internal waves generated by geostrophic motions over small scale topography. *Ocean Science*, submitted.

Naveira-Garabato, A. C. N., Polzin, K. L., King, B. A., and Heywood, K. J. and Visbeck, M. (2004). Widespread intense turbulent mixing in the southern ocean. *Science*, 303:210–213.

Nikurashin, M. and Ferrari, R. (2010). Radiation and dissipation of internal waves generated by geostrophic motions impinging on small-scale topography. *J. Phys. Oceanography*, 40:1055–1074.

Nikurashin, M., Vallis, G., and Adcroft, A. (2013). Routes to energy dissipation for geostrophic flows in the Southern Ocean. *Nature Geoscience*, 6:48–51.

Sheppard, P. A. (1956). Airflow over mountains. *Quart. J. Roy. Meteor. Soc.*, 82:528–529.

Sous, D., Sommeria, J., and Boyer, D. (2013). Friction law and turbulent properties in a laboratory Ekman boundary layer. *Physics of Flyids*, 25:046602.

Voisin, B. (2007). Lee waves from a sphere in a stratified flow. *J. Fluid Mech.*, 574:273–315.